

Self-guided beams in low-birefringence nematic liquid crystals

Michał Kwasny,¹ Urszula A. Laudyn,¹ Filip A. Sala,¹ Alessandro Alberucci,² Mirosław A. Karpierz,¹ and Gaetano Assanto²

¹*Faculty of Physics, Warsaw University of Technology, Koszykowa 75, 00-662 Warsaw, Poland*

²*Nonlinear Optics and Optoelectronics Lab (NooEL), Via della Vasca Navale 84, 00146 Rome, Italy*

(Received 27 April 2012; published 17 July 2012)

We investigate the nonlinear propagation of coherent light beams in planar samples of low-birefringence nematic liquid crystals, changing the input polarization and the incidence angle in order to enhance reorientational self-focusing and generate optical spatial solitons under a variety of previously unexplored launch conditions. We find that reorientational spatial solitons require larger excitation powers in low-birefringence than in high-birefringence nematic liquid crystals but remain stable. We compare the experimental results with full-vectorial numerical simulations.

DOI: [10.1103/PhysRevA.86.013824](https://doi.org/10.1103/PhysRevA.86.013824)

PACS number(s): 42.65.Tg, 42.25.Lc, 42.70.Df

I. INTRODUCTION

Beam self-confinement is one of the most striking phenomena in nonlinear optics: the spreading of an optical wave packet upon diffraction is counteracted by nonlinear self-focusing in transverse space. The mutual compensation of these two effects in Kerr media can support optical spatial solitons at a critical excitation, but can give rise to self-trapped beams or solitary waves in a larger class of dielectrics where the nonlinear polarization exhibits a nontrivial dependence on the input power (e.g., saturation, nonlocality, multiphoton absorption, etc.). In optics the terms spatial solitary waves and solitons are often used interchangeably [1–3]. Solitons are a core topic in nonlinear physics due to their ubiquitous character: they were first reported in fluids [4] and later observed in solid state physics, chemistry, Bose-Einstein condensates, plasmas, etc. [5–9].

Optical spatial solitons (we will omit optical and spatial hereafter) are most often studied in dielectrics where the refractive index increases depending on the intensity of light [1–3,10]. In such media, they self-confine by generating a graded index profile which is a waveguide, the latter supporting the soliton as a mode and, depending on wavelength and polarization, capable of trapping other (weaker) signals of different wavelengths; solitons have therefore been considered as basic elements in all-optical circuits for signal processing, switching, and re-addressing in future generations of light-controlled information handling [11]. Solitons have been demonstrated and investigated in photorefractive crystals [12,13], atomic vapors [14], soft matter [15], glasses [16,17], semiconductors [18], Bose-Einstein condensates [19], and nematic liquid crystals (NLCs) [20,21], among others. Solitons in NLCs, also known as nematons [21,22], have attracted a great deal of attention in the last few years for several reasons: the large nonlinearity stemming from molecular reorientation [23], the highly nonlocal response able to stabilize them in two transverse dimensions [24], and the significant electro-optic effect allowing to control their trajectory [25–28]. To date, nematons have been studied in several geometries [22], including planar [20,29–32], homeotropic [33], and twisted and chiral NLCs [34–37].

When the average orientation (i.e., the director \hat{n}) of the elongated NLC molecules is with the long axis (i.e., the optic axis of the corresponding uniaxial) perpendicular to the

electric field, reorientation occurs at optical intensities above a threshold; the so-called Fréedericksz transition [23,38]. The latter can be avoided by either applying external voltage(s) to tilt the director [20,21] or by rubbing the cell interfaces to align the director at an arbitrary initial angle in the principal plane of the propagating electric field of the beam [25,27,28]. In all cases, the mutual orientation of molecular director and electric field vector affects the medium anisotropy and nonlinearity [39–42], hence the excitation level and polarization required for nematonic generation. Since self-focusing in uniaxial reorientational NLCs stems from the increase in extraordinary refractive index due to the reorientation of the optic axis (i.e., molecular director \hat{n}), the birefringence $\Delta n = n_e - n_o$ (i.e., the index dynamics available upon rotation of \hat{n} in the principal plane of propagation) is expected to play an important role on the formation of nematons.

In this work we study nematonic propagation in planarly oriented samples of low-birefringence NLCs, varying the input beam polarization and the direction of its wave vector \mathbf{k} . By comparing the experimental results with numerical simulations using a vectorial beam propagator, we identify the best parameters for light self-trapping and gain insight in the reorientational response of NLCs for arbitrary launch conditions.

II. SAMPLE

The sample is sketched in Figs. 1(a) and 1(b). The planar cell consists of two parallel glass plates glued together with a separation $d = 60 \mu\text{m}$, filled with the low birefringence nematic liquid crystal 1110, with $n_o = n_{\perp} = 1.45$ and $n_e = n_{\parallel} = 1.49$ at room temperature and at $1.064 \mu\text{m}$ [43]. The director is aligned along y by properly treating the inner interface of each glass plate. A Nd:YAG laser beam ($\lambda = 1064 \text{ nm}$), linearly polarized with electric field at angle φ with respect to y in the xy plane, is focused at the cell entrance with an input waist $w_0 = 3.8 \mu\text{m}$ by a $20\times$ microscope objective and launched with wave vector \mathbf{k} at angles $0 < \alpha < \pi/4$ with respect to the z axis. In the uniaxial NLC, ordinary and extraordinary wave vectors form angles α_o and α_e with z , respectively, owing to the different refractive indices [Fig. 1(c)]. The extraordinary Poynting vector points at $\alpha_e + \delta$, with δ being the walk off [Fig. 1(d)]. The propagating beam

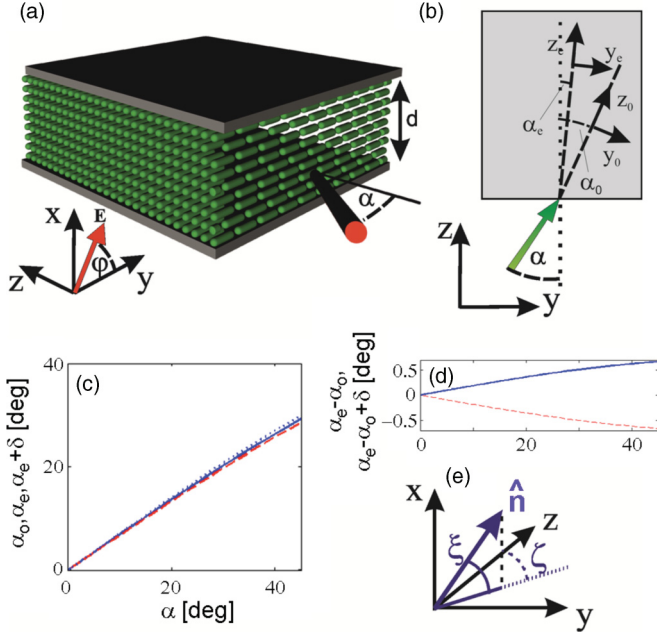


FIG. 1. (Color online) (a) Geometry of NLC sample. The input beam is linearly polarized with electric field at angle φ and propagates with wave vector \mathbf{k} at an angle α_0 with respect to z ; (b) Top view (yz plane); director of ordinary and extraordinary wave vectors and corresponding reference frames y_0z_0 and y_ez_e , respectively. (c) α_0 (solid blue line) and α_e (red dashed line) versus incidence angle α , as determined by the Snell law; the blue dotted line represents the extraordinary ray with walk off. (d) Walk off between ordinary and extraordinary Poynting vectors (blue solid line) and double refraction $\alpha_e - \alpha_0$ (red dashed line) versus incidence angle α . (e) Polar angles describing the director \hat{n} .

is imaged with a high-resolution silicon CCD collecting the photons scattered out of the yz plane.

III. MODEL

Nonlinear light propagation in NLCs is governed by Maxwell equations coupled with the Euler-Lagrange equations determining the director distribution and stemming from the minimization of the NLC energy, with both elastic and optical contributions [38]. The relative dielectric permittivity of uniaxial NLC can be cast in the form $\varepsilon_{jk} = \varepsilon_{\perp} \delta_{jk} + \varepsilon_a n_j n_k$ ($j, k = x, y, z$), with $\varepsilon_a = (n_{\parallel}^2 - n_{\perp}^2)$ being the optical anisotropy, δ_{jk} being the Kronecker delta, and n_j being the Cartesian components of the director \hat{n} [38].

Depending on the excitation beam (see Fig. 1), reorientation can lead to the director rotation in three dimensions (3D), as described by the two polar angles ξ and ζ [see Fig. 1(e)]; that is, $\hat{n} = (\sin \xi, \cos \xi \sin \zeta, \cos \xi \cos \zeta)$ in the xyz reference frame. An intense beam can give rise to a spatially inhomogeneous Coulombian torque, with a corresponding director distribution continuously varying across the cell. Such distribution of both ξ and ζ can result in coupling between ordinary and extraordinary components of the wave, even in the paraxial regime [44]. The director rotation reduces to a simpler planar rotation for either $\varphi = 0$ or $\alpha = 0$. The first case, $\varphi = 0$, corresponds to an input electric field lying

in the plane yz : for any α the director can rotate in yz , maintaining $\xi = 0$. In this limit the only excited wave is extraordinary, with magnetic field $\mathbf{H}_e = A_e \exp(ik_0 n_e^{(b)} z_e) \hat{x}$, with A_e being the slowly varying envelope, k_0 being the wave vector in vacuum, and $n_e^{(b)}$ being the carrier refractive index: this configuration has been extensively studied in the literature and light propagation in the paraxial limit is ruled by [39]

$$2ik_0 n_e^{(b)} \left(\frac{\partial A_e}{\partial z_e} + \tan \delta^{(b)} \frac{\partial A_e}{\partial y_e} \right) + D_y \frac{\partial^2 A_e}{\partial y_e^2} + \frac{\partial^2 A_e}{\partial x_e^2} + k_0^2 \Delta n_e^2 A_e = 0, \quad (1)$$

$$\nabla^2 \zeta + \gamma \left(\frac{Z_0}{n_e^{(b)} \cos \delta^{(b)}} \right)^2 |A_e|^2 \sin[2(\theta - \delta^{(b)})] = 0, \quad (2)$$

with $\theta = \zeta - \alpha_e$, $\delta^{(b)}$ being the local walk off, Z_0 being the vacuum impedance, D_y being the diffraction coefficient along y , and Δn_e^2 being the nonlinear index well due to reorientation. In the reorientational equation (2) we introduced the interaction strength $\gamma = \varepsilon_0 \varepsilon_a / (4K)$, with K being a single-valued (scalar) Frank elastic constant. By combining Eqs. (1) and (2) we can define an effective nonlocal Kerr coefficient n_2 :

$$n_2 = 2\gamma n_e^2(\theta_0) \tan \delta_0 \sin[2(\theta_0 - \delta_0)], \quad (3)$$

where δ_0 is the walk off corresponding to $\theta_0 = \pi/2 - \alpha_e$. The scalar coefficient n_2 depends only on the initial angle θ_0 between beam wave vector and molecular director and on the optical properties (that is, ε_{\parallel} and ε_{\perp}) of the dielectric [39]. In the limit of small anisotropy (i.e., $\varepsilon_{\parallel} \approx \varepsilon_{\perp}$), Eq. (3) yields [45]

$$n_2 = (\varepsilon_0 \varepsilon_a^2 / 4K) \sin[2(\theta_0 - \delta_0)] \sin(2\theta_0). \quad (4)$$

In the second case, $\alpha = 0$, the beam impinges orthogonally to the sample: ordinary (\mathbf{k}_o) and extraordinary (\mathbf{k}_e) wave vectors are both parallel to z and the director can rotate in the xy plane, with $\zeta = \pi/2$ and ξ free to vary. When the input power is high enough to induce a nonlinear rotation, ordinary and extraordinary waves get coupled through the inhomogeneous distribution of the optic axis [46]. A similar configuration was previously analyzed experimentally in the (1+1)D case [47]. Light propagation can be modeled in terms of its transverse electric field as

$$\left(1 - \frac{\varepsilon_{yy}}{\varepsilon_{zz}}\right) \frac{\partial^2 E_y}{\partial x \partial y} - \frac{\varepsilon_{xy}}{\varepsilon_{zz}} \frac{\partial^2 E_y}{\partial x^2} - \frac{\varepsilon_{xx}}{\varepsilon_{zz}} \frac{\partial^2 E_x}{\partial x^2} - \frac{\partial^2 E_x}{\partial y^2} - \frac{\partial^2 E_x}{\partial z^2} - \frac{\varepsilon_{xy}}{\varepsilon_{zz}} \frac{\partial^2 E_x}{\partial x \partial y} = k_0^2 (\varepsilon_{xx} E_x + \varepsilon_{xy} E_y), \quad (5)$$

$$\left(1 - \frac{\varepsilon_{xx}}{\varepsilon_{zz}}\right) \frac{\partial^2 E_x}{\partial x \partial y} - \frac{\varepsilon_{xy}}{\varepsilon_{zz}} \frac{\partial^2 E_x}{\partial y^2} - \frac{\varepsilon_{yy}}{\varepsilon_{zz}} \frac{\partial^2 E_y}{\partial y^2} - \frac{\partial^2 E_y}{\partial x^2} - \frac{\partial^2 E_y}{\partial z^2} - \frac{\varepsilon_{xy}}{\varepsilon_{zz}} \frac{\partial^2 E_y}{\partial x \partial y} = k_0^2 (\varepsilon_{yy} E_y + \varepsilon_{xy} E_x), \quad (6)$$

$$\nabla^2 \xi + \gamma [(|E_x|^2 - |E_y|^2) \sin(2\xi) + 2\text{Re}(E_x E_y^*) \cos(2\xi)] = 0, \quad (7)$$

with E_x and E_y being the components of the electric field along x and y , respectively.

From Eqs. (5) and (6) it is apparent that the electric field components along x and y are entangled: in fact, ordinary and

extraordinary waves can only be defined locally, due to the transverse distribution of the optic axis. It is noteworthy that the walk off is zero and there are no first-order derivatives with respect to the propagation coordinate z . From Equation (7), at the input $z = 0$ the torque is proportional to $\gamma \sin(2\varphi)$: hence, it is maximum for $\varphi = \pi/4$; for $\varphi = \pi/2$ (i.e., input field parallel to x) reorientation can only occur above a threshold [48].

In low-birefringence NLCs (i.e., for the mixture 1110 used in our experiments, with $\Delta n = n_{\parallel} - n_{\perp} = 0.04$), the power required for self-trapping is higher than in other NLCs [39], [45], including cholesterics [36,37]. In fact, according to Eq. (3), the index well is approximately proportional to the square of the birefringence Δn , as the induced dipoles are proportional to Δn and so is the nonlinear index for a given reorientation [45]. Moreover, the Frank elastic constants of the mixture 1110 are 2 to 3 times larger than in the commonly employed nematic 5CB and E7; therefore, n_2^{1110} is expected to be about $8 \div 12$ times smaller than $n_2^{E7} \cong n_2^{5CB}$, leading to a power requirement for nematicons in 1110 about one order of magnitude higher than in E7, depending on input polarization (φ) and incidence angle (α). Low birefringence also leads to small walk off, with a maximum $\delta = 1.6^\circ$ in 1110 compared to $\delta = 7^\circ$ in E7 at $\lambda = 1064$ nm. Finally, reduced scattering and random index fluctuations in low-birefringence 1110 allow us to obtain stable nematicons in spite of the higher required excitations as compared to high-birefringence NLCs.

IV. EXPERIMENTAL RESULTS

A. Normal incidence, $\alpha = 0$

We first examine the case of normal incidence. Figure 2 displays a few examples of beams launched in 1110 for

$\alpha = 0$ and $\varphi = \pi/4$: at powers P below $\cong 70$ mW diffraction prevails over self-focusing [Figs. 2(a) and 2(b)], even though it progressively reduces as power increases. Nematicons are obtained for $P \geq 100$ mW and propagate for over 50 Rayleigh lengths ($L_R \approx 42 \mu\text{m}$), with waist oscillations along z [see Fig. 2(b)] consistent with the breathing character of nonlocal solitons [49]. When light is polarized along x ($\varphi = \pi/2$), a threshold effect linked to the optical Fréedericksz transition [see Fig. 2(c)] leads to nematicon generation only above 120 mW [50]. Conversely, when the beam is polarized along y ($\varphi = 0$), the torque is zero and no reorientation takes place, with beams diffracting for excitations up to 160 mW and no evidence of self-focusing, confirming the negligible role of thermal effects [51]. Summarizing, the discussed nonlinear effects are reorientational and maximum for $\varphi \approx \pi/4$. The reorientational self-focusing we observed stems from an *effective* index well (waveguide) due to the continuous power exchange between ordinary and extraordinary components, in analogy to what was previously reported in a (1+1)D geometry [47].

B. Oblique incidence

We now turn to the case $\alpha \neq 0$. As α increases starting from normal incidence, self-confinement for $\varphi = \pi/4$ occurs at lower and lower powers [Figs. 3(b)–3(d)] and is optimized for $\alpha = \pi/4$ [Fig. 3(d)]. When $\alpha = \pi/4$, axes z and z_0 form a relative angle of about 29° due to refraction at the air-NLC interface [see Fig. 1(c)]. Angles $\alpha > \pi/4$ could not be tested in our experiments due to difficulties in injecting light in the NLC sample.

We compared the experimental results with numerical simulations using a fully vectorial code based on the beam

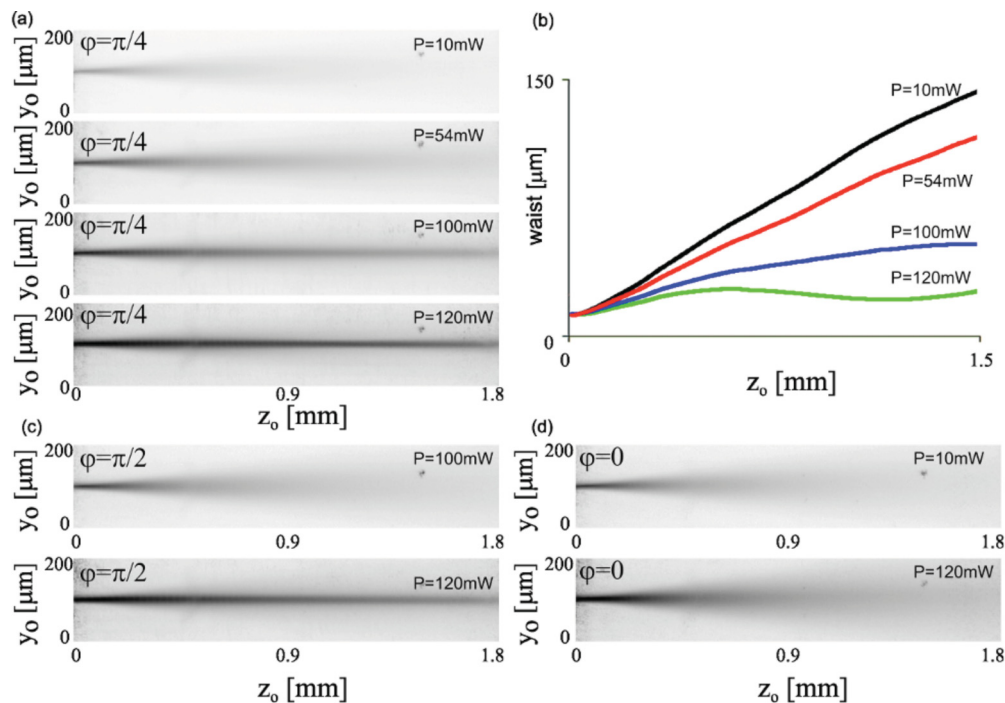


FIG. 2. (Color online) (a) Measured beam evolution in the $y_0 z_0$ plane for several input powers, $\alpha = 0$ and $\varphi = \pi/4$. (b) Measured beam waist versus z_0 corresponding to the cases in (a). Beam propagation for $\alpha = 0$ and (c) $\varphi = \pi/2$, (d) $\varphi = 0$.

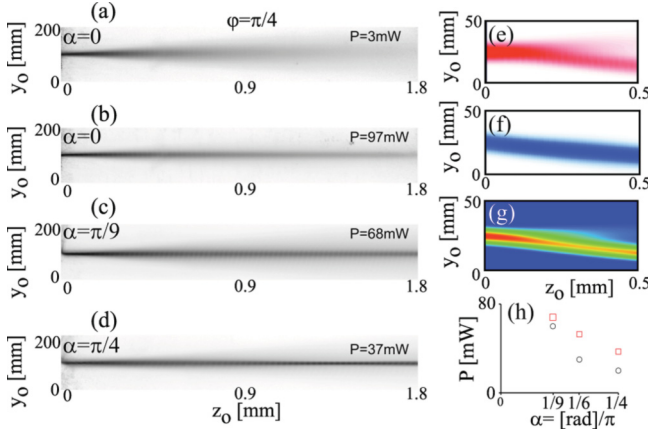


FIG. 3. (Color online) Experimental results on beam propagation in the (a) linear and (b)–(d) nonlinear regimes. A linearly polarized input beam is launched with $\varphi = \pi/4$ at various α . Numerical simulation of a beam propagating for $\alpha = \pi/4$ and $\varphi = \pi/4$: evolution in the plane $y_0 z_0$ of (e) $|E_x|^2$, (f) $|E_y|^2$, and (g) the corresponding total intensity $|E_x|^2 + |E_y|^2$. (h) Minimum beam power versus α for nonlinear self-collimation with $\varphi = \pi/4$: calculated (black circles) and measured (red squares) values.

propagation method. For the sake of simplicity, the simulations were carried out considering the wave vector parallel to z_0 but the director (at rest) at angle $-\alpha_e$ with z_0 ; such geometry corresponds to our experimental conditions in the limit of negligible misalignment between ordinary and extraordinary wave vectors [as in our case; see Fig. 1(c)] and a negligible role of the input interface on reorientation. The minimum nematicon power was calculated for various input angles α and linear polarization fixed at $\varphi = \pi/4$ [Fig. 3(h)]; in agreement with experimental data, the self-trapping power is maximum for $\alpha = 0$ and minimum for $\alpha = \pi/4$, with discrepancies between experimental and numerical values

mainly due to insertion and propagation losses (not included in the simulations). A detailed numerical study of the beam evolution for $\alpha = \pi/4$ is shown in Figs. 3(e)–3(g): the overall beam tends to travel at a finite walk off, although its x and y components exchange energy during propagation, leading to a diffractive (weaker) background (along z_0) associated with the ordinary wave and to a solitary wave in which both components tend to remain trapped. Such numerical results on mixed-polarization self-trapping with a diffractive background are in agreement with the experimental observations [Fig. 3(d)].

Figure 4 shows the evolution of a beam launched for $\alpha = \pi/4$ and three input polarizations φ (photos in the $y_0 z_0$ reference system). For light polarized along y ($\varphi = 0$) a spatial solitary wave is obtained at $P = 30$ mW. Reorientation takes place in the $y_0 z_0$ plane according to Eqs. (1) and (2) and nematicons remain stable for powers up to 120 mW. Slightly increasing the input power modifies the beam trajectory due to nonlinear changes in walk off [40,52]: in $z_0 = 1.5$ mm the beam shifts laterally by about $10 \mu\text{m}$ along y_0 for excitations increasing from 30 to 120 mW.

For light polarized along x ($\varphi = \pi/2$) self-focusing is too weak to induce self-confinement for $P = 30$ mW and $P = 38$ mW [Figs. 4(a) and 4(b); dotted lines in Figs. 4(c) and 4(d)]. Above 150 mW the electric field is intense enough to overcome the Fréedericksz threshold and form a temporally unstable nematicon, as thermo-optic effects cause the material to undergo convective motion and molecular disorder. A higher value of the optical Fréedericksz threshold with respect to the case $\alpha = 0$ is ascribed to larger insertion losses at the input interface, as reflection gets larger with α [53].

For light polarized at $\varphi = \pi/4$ and power $P = 30$ mW the diffractive background is visible in Fig. 4(a), owing to the power coupled to the ordinary wave; the extraordinary component is less confined than in the case $\varphi = 0$ and $P = 30$ mW due to the smaller fraction of the excitation

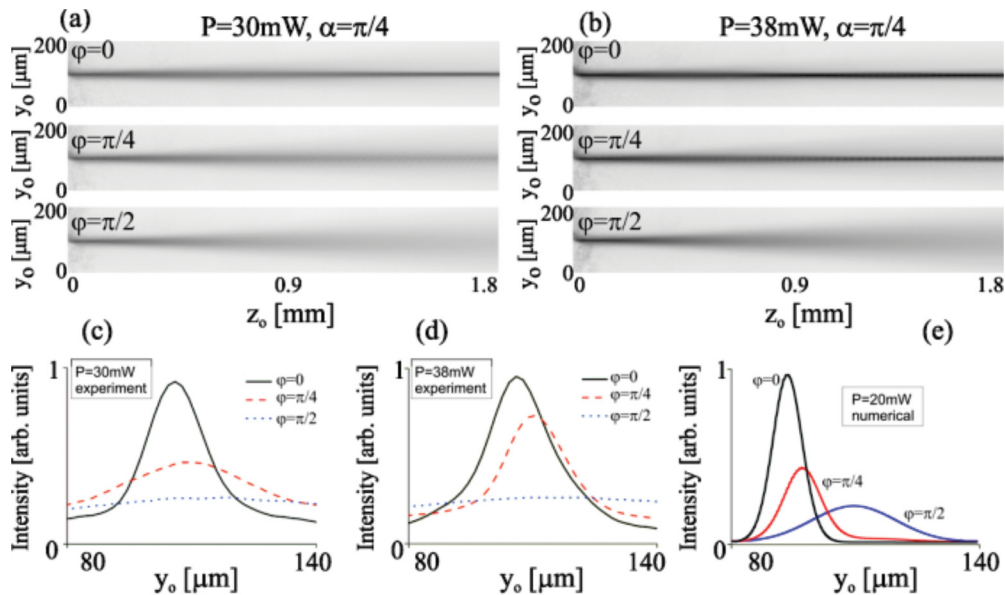


FIG. 4. (Color online) Experimental results on beam propagation for $\alpha = \pi/4$ and various input polarizations (legends) and powers: (a) $P = 30$ mW; (b) $P = 38$ mW. Panels (c) and (d) show beam profiles at a distance of $z_0 = 1.5$ mm. (e) Profiles calculated for $P = 20$ mW and $\alpha = \pi/4$ in $z_0 = 0.5$ mm.

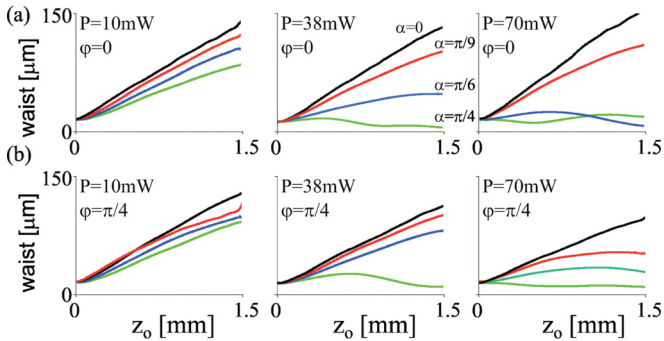


FIG. 5. (Color online) (a) Measured beam waist w versus propagation distance z_0 for $\varphi = 0$, various excitations ($P = 10, 38$, and 70 mW, respectively) and angles α . (b) Corresponding waist versus z for light polarized at $\varphi = \pi/4$; lines from top to bottom correspond to $\alpha = 0$ (black), $\pi/9$ (red), $\pi/6$ (blue), $\pi/4$ (green).

coupled to the y polarization. For input power >38 mW a net increase in self-focusing is observed [Fig. 4(d)]. The measured displacement across y_0 is about $15 \mu\text{m}$ [$z_0 = 1.5$ mm, dashed lines in Figs. 4(c) and 4(d)]. Accounting for blurring from scattering [49], the measured nematicon widths are approximately $10 \mu\text{m}$ larger than the actual waist and the experimental results are in good agreement with numerical calculations for $\alpha = \pi/4$ and $P = 20$ mW [Fig. 4(e)].

The results on self-focusing for different polarizations φ and propagation angles α are summarized in Figs. 5(a) and 5(b). Figure 5(a) shows the measured beam waist versus z for $\varphi = 0$, corresponding to the case modelled by Eqs. (1) and (2): as predicted by Eq. (3) the nonlinear effects are maximum when $\theta_0 = \pi/2 - \alpha_e$ between wave vector and director is close to $\pi/4$, in agreement with Ref. [39]. The

latter dependence holds valid for the case $\varphi = \pi/4$, as well [Fig. 5(b)], but with the beam undergoing a weaker self-trapping than in the case $\varphi = 0$ (fixed power) owing to the lower power coupled to the extraordinary wave.

V. CONCLUSIONS

In conclusion, nematicons were observed in low-birefringence nematic liquid crystals over propagation distances of 2 mm and powers of a few tens of mW. We observed (2 + 1)D self-confined optical waves excited by combined ordinary and extraordinary polarizations. We demonstrated that maximum self-focusing occurs when the beam wave vector is at an angle of $\alpha_e = \pi/4$ with respect to the director at rest (i.e., in the absence of illumination), independently on the input polarization φ . Moreover, we found that, if the input polarization is not parallel to the director at rest (corresponding to the case $\alpha = 0$ discussed above), self-focusing is maximum when the input polarization couples all the power to an extraordinary wave (i.e., for $\varphi = 0$). Finally, compared with nematicons in high-birefringence NLCs, nematicons in low-birefringence NLC require larger excitations but—despite them—remain temporally stable.

ACKNOWLEDGMENTS

The authors thank Dr. E. Nowinowski-Kruszelnicki for sample preparation and Dr. M. Sierakowski for enlightening discussions and collaboration. This work was partially supported by the National Science Centre. Partial support in Italy was provided by a NATO-EOARD (European Office of Aerospace Research and Development) grant as well as financial help from Regione Lazio.

- [1] *Spatial Solitons*, edited by S. Trillo and W. Torruellas (Berlin, Springer Verlag, 2001).
- [2] Y. Kivshar and Agrawal, *Optical Solitons* (Academic, San Diego, 2003).
- [3] C. Conti and G. Assanto, *Nonlinear Optics Applications: Bright Spatial Solitons*, in *Encyclopedia of Modern Optics*, edited by R. D. Guenther, D. G. Steel, and L. Bayvel (Elsevier, Oxford, 2004), Vol. 5, pp. 43–55.
- [4] J. S. Russell, *Report on the 14th Meeting of the British Association for the Advancement of Science* (Murray, London, 1844), p. 311.
- [5] Y. Togawa, T. Koyama, K. Takayanagi, S. Mori, Y. Kousaka, J. Akimitsu, S. Nishihara, K. Inoue, A. S. Ovchinnikov, and J. Kishine, *Phys. Rev. Lett.* **108**, 107202 (2012).
- [6] L. Khaykovich, F. Schreck, G. Ferrari, T. Bourdel, J. Cubizolles, L. D. Carr, Y. Castin, and C. Salomon, *Science* **296**, 1290 (2002).
- [7] Y. Nakamura and I. Tsukabayashi, *Phys. Rev. Lett.* **52**, 2356 (1984).
- [8] T. Dauxois and M. Peyrard, *Physics of Solitons* (Cambridge University Press, Cambridge, 2006).
- [9] *Localized States in Physics: Solitons and Patterns*, edited by O. Descalzi, M. Clerc, S. Residori, and G. Assanto (Springer, Berlin, 2011).
- [10] G. I. Stegeman and M. Segev, *Science* **286**, 1518 (1999).
- [11] A. D. Boardman and A. P. Sukhorukov, *Soliton Driven Photonics* (Kluwer Academic, Dordrecht, 2001).
- [12] G. C. Duree, J. L. Shultz, G. J. Salamo, M. Segev, A. Yariv, B. Crosignani, P. Di Porto, E. J. Sharp, and R. R. Neurgaonkar, *Phys. Rev. Lett.* **71**, 533 (1993).
- [13] S. Jia, J. Lee, J. W. Fleischer, G. A. Siviloglou, and D. N. Christodoulides, *Phys. Rev. Lett.* **104**, 253904 (2010).
- [14] D. Suter and T. Blasberg, *Phys. Rev. A* **48**, 4583 (1993).
- [15] P. J. Reece, E. M. Wright, and K. Dholakia, *Phys. Rev. Lett.* **98**, 203902 (2007).
- [16] A. Pasquazi, S. Stivala, G. Assanto, J. Gonzalo, and J. Solis, *Phys. Rev. A* **77**, 043808 (2008).
- [17] C. Rotschild, O. Cohen, O. Manela, M. Segev, and T. Carmon, *Phys. Rev. Lett.* **95**, 213904 (2005).
- [18] L. Friedrich, G. I. Stegeman, P. Millar, C. J. Hamilton, and J. S. Aitchison, *Opt. Lett.* **23**, 1438 (1998).
- [19] G. Labeyrie and U. Bortolozzo, *Opt. Lett.* **36**, 2158 (2011).
- [20] M. Peccianti, G. Assanto, A. De Luca, C. Umeton, and I. C. Khoo, *Appl. Phys. Lett.* **77**, 7 (2000).
- [21] G. Assanto and M. A. Karpierz, *Liq. Cryst.* **36**, 1161 (2009).
- [22] M. Peccianti and G. Assanto, *Phys. Rep.* **516**, 147 (2012).

- [23] I. C. Khoo, *Phys. Rep.* **471**, 221 (2009).
- [24] C. Conti, M. Peccianti, and G. Assanto, *Phys. Rev. Lett.* **91**, 073901 (2003).
- [25] M. Peccianti, C. Conti, G. Assanto, A. De Luca, and C. Umeton, *Nature (London)* **432**, 733 (2004).
- [26] M. Peccianti, A. Dyadyusha, M. Kaczmarek, and G. Assanto, *Nat. Phys.* **2**, 737 (2006).
- [27] A. Piccardi, M. Peccianti, G. Assanto, A. Dyadyusha, and M. Kaczmarek, *Appl. Phys. Lett.* **94**, 091106 (2009).
- [28] A. Alberucci, A. Piccardi, U. Bortolozzo, S. Residori, and G. Assanto, *Opt. Lett.* **35**, 390 (2010).
- [29] M. Peccianti, K. A. Brzdańkiewicz, and G. Assanto, *Opt. Lett.* **27**, 1460 (2002).
- [30] G. Assanto, A. Fratalocchi, and M. Peccianti, *Opt. Express* **15**, 5248 (2007).
- [31] J. Beeckman, K. Neyts, X. Hutsebaut, C. Cambournac, and M. Haelterman, *Opt. Express* **12**, 1011 (2004).
- [32] Y. V. Izdebskaya, A. S. Desyatnikov, G. Assanto, and Y. S. Kivshar, *Opt. Express* **19**, 21457 (2011).
- [33] M. A. Karpierz, M. Sierakowski, M. Swillo, and T. R. Woliński, *Mol. Cryst. Liq. Cryst.* **320**, 157 (1998).
- [34] M. A. Karpierz, M. Sierakowski, and T. R. Woliński, *Mol. Cryst. Liq. Cryst.* **375**, 313 (2002).
- [35] K. Jaworowicz, K. A. Brzdańkiewicz, M. A. Karpierz, and M. Sierakowski, *Mol. Cryst. Liq. Cryst.* **453**, 301 (2006).
- [36] U. A. Laudyn, M. Kwasny, and M. A. Karpierz, *Appl. Phys. Lett.* **94**, 091110 (2009).
- [37] U. A. Laudyn, M. Kwasny, and M. A. Karpierz, *Mol. Cryst. Liq. Cryst.* **527**, 92 (2010).
- [38] F. Simoni, *Nonlinear Optical Properties of Liquid Crystals and Polymer Dispersed Liquid Crystals* (World Scientific, Singapore, 1997).
- [39] A. Alberucci, A. Piccardi, M. Peccianti, M. Kaczmarek, and G. Assanto, *Phys. Rev. A* **82**, 023806 (2010).
- [40] A. Piccardi, A. Alberucci, and G. Assanto, *Appl. Phys. Lett.* **96**, 0611005 (2010).
- [41] Y. V. Izdebskaya, V. G. Shvedov, A. S. Desyatnikov, W. Z. Krolikowski, M. Belic, G. Assanto, and Y. S. Kivshar, *Opt. Express* **18**, 3258 (2010).
- [42] M. Peccianti and G. Assanto, *Opt. Lett.* **30**, 2290 (2005).
- [43] 1110 nematic mixture synthesized by Professor R. Dabrowski at the Military University of Technology in Warsaw.
- [44] M. Lax, W. H. Louisell, and W. B. McKnight, *Phys. Rev. A* **11**, 1365 (1975).
- [45] A. Piccardi, M. Trotta, M. Kwasny, A. Alberucci, R. Asquini, M. Karpierz, A. D'Alessandro, and G. Assanto, *Appl. Phys. B* **104**, 805 (2011).
- [46] L. Marrucci, C. Manzo, and D. Paparo, *Phys. Rev. Lett.* **96**, 163905 (2006).
- [47] M. A. Karpierz, *Phys. Rev. E* **66**, 036603 (2002).
- [48] S. D. Durbin, S. M. Arakelian, and Y. R. Shen, *Phys. Rev. Lett.* **47**, 1411 (1981).
- [49] C. Conti, M. Peccianti, and G. Assanto, *Phys. Rev. Lett.* **92**, 113902 (2004).
- [50] E. Braun, L. P. Faucheux, and A. Libchaber, *Phys. Rev. A* **48**, 611 (1993).
- [51] M. Warengem, J. F. Blach and J. F. Henninot, *J. Opt. Soc. Am. B* **25**, 1882 (2008).
- [52] A. Piccardi, A. Alberucci, and G. Assanto, *J. Opt. Soc. Am. B* **27**, 2398 (2010).
- [53] M. Born and E. Wolf, *Principle of Optics* (Pergamon Press, New York, 1975).